Narrowband four-photon states from spontaneous four-wave mixing

Yifan Li,[1] Justin Yu Xiang Peh,[1] Chang Hoong Chow,[1] Boon Long Ng,[1] Vindhiya Prakash,[1] and Christian Kurtsiefer[1,2]

[1] *Centre for Quantum Technologies, National University of Singapore, 3 Science Drive 2, Singapore 117543*
[2] *Department of Physics, National University of Singapore, 2 Science Drive 3, Singapore 117551**

We observe time-correlated four photons within a correlation window of 20 ns from spontaneous four-wave mixing via a double-Λ scheme in a cold cloud of ^{87}Rb atoms. In contrast to high-power pulsed pumping of $\chi^{(2)}$ nonlinear processes in crystals, our scheme generates correlated four-photon states by direct continuous-wave pumping at nominal powers. We verify the presence of genuinely correlated four-photon states over accidentals by higher-order intensity cross-correlation measurements and accidental subtraction. We infer a time-correlated four-photon generation rate of $2.5(4) \times 10^6$ counts per second close to saturation. The photons produced are near-resonant with atomic transitions, and have a bandwidth in the order of MHz, making them readily compatible with quantum networking applications involving atoms.

Multiphoton states, i.e., states with more than two photons entangled or correlated across single or multiple modes, are extremely useful resources for quantum sciences and technologies [1]. At a foundational level, multiphoton Greenberger–Horne–Zeilinger (GHZ) states and W states have enabled powerful tests to disprove local realistic theories [2, 3] and explore unique entanglement classes [4, 5]. Multiphoton states enable secure communication protocols [6, 7] and also find applications in quantum metrology [8]. In the form of cluster states, they are essential for scalable and resource-efficient photonic quantum computing [9, 10]. States with four photons have also been used to encode decoherence-resistant quantum information [11].

It is well known that some multiphoton states can be directly produced by strong pumping of non-linear processes like spontaneous parametric downconversion (SPDC), where the probability of producing more than one photon pair increases with the pump power [12, 13]. In directly pumping an SPDC process, the probability of producing entangled four photons is twice as high as producing two independent entangled pairs [14, 15]. Highly entangled W states have also been obtained from the higher-order component in a directly pumped SPDC process [16].

Photons from SPDC typically have large bandwidths and correspondingly short coherence lengths, often shorter than the length of the downconversion crystal itself. Thus, in the above cases, pulsed pumps with large instantaneous powers and narrowband filters are often used to isolate and analyze correlated multiphoton states from SPDC. This leads to losses. Direct filter-free analysis of the rich temporal structure of higher-order correlated photons from SPDC [17] has been challenging due to the jitter and response averaging of detectors [18]. The large bandwidth of photons from SPDC also limits their use in quantum memory and repeater schemes that require efficient interfacing with material quantum systems.

Here, we demonstrate a bright source for narrowband time-correlated photon quadruplets, matched to atomic transitions, based on direct continuous-wave (cw) pumping of spontaneous four-wave mixing (SFWM) in a cold atomic cloud. In atomic clouds, SFWM is an excellent and bright [19–21] alternative to SPDC for producing narrowband photon pairs with long coherence times [22–26]. Photons from this process can be spectrally shaped to be narrower or wider than atomic transition linewidths, making them well-suited for quantum networking applications [27], such as memory, repeater [28], and entanglement distribution schemes involving atoms. Furthermore, their long coherence times, typically in the order of tens of nanoseconds, allow them to be well-resolved by off-the-shelf photon detection electronics.

We study correlated photon quadruplets from SFWM in a cold cloud of rubidium atoms using Hanbury Brown and Twiss (HBT) type setups, one in each of the correlated modes. We introduce an efficient technique for identifying three-fold and four-fold coincidences of the photons generated from the nonlinear interaction. We analyze the temporal distribution of the detected triplet and quadruplet coincidences, and observe that photon pairs bunch together in both measurements within a correlation window of 20 ns. The aggregate coincidences detected within this window is significantly larger than the sum of accidentals detected at longer delays, indicating a strong contribution from quadruplets correlated in time, over accidental/uncorrelated four-photon states.

In detail, our scheme is based on SFWM using a double-Λ configuration of energy levels in a cold cloud of ^{87}Rb atoms, similar to the systems reported in [24, 29]. The SFWM process is driven by a weak cw pump (of frequency ω_p) detuned by Δ_p from $|5S_{1/2}, F = 1\rangle \rightarrow |5P_{3/2}, F' = 2\rangle$ and a strong cw coupling laser (of frequency ω_c) resonant to the $|5S_{1/2}, F = 2\rangle \rightarrow |5P_{1/2}, F' = 2\rangle$ transition. Nonlinear interaction of the pump and coupling fields with the atomic medium generates correlated optical fields called Stokes and anti-Stokes by convention. The Stokes photons are generated at a frequency ω_s close to the $|5P_{3/2}, F' = 2\rangle \rightarrow |5S_{1/2}, F = 2\rangle$ tran-

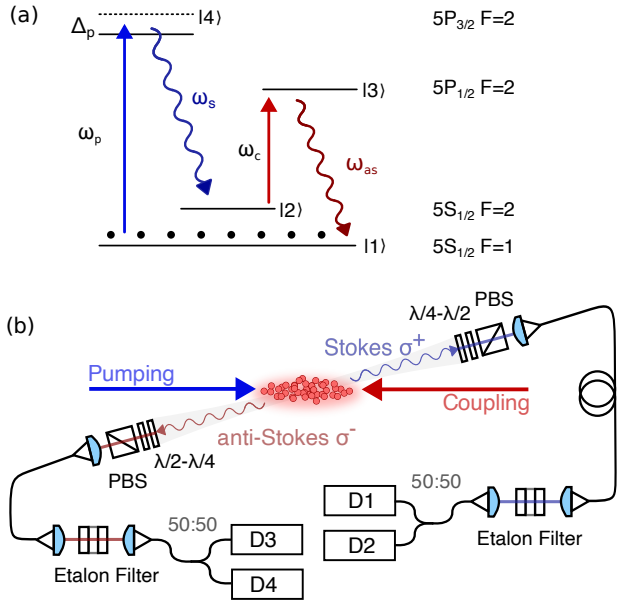

FIG. 1. (a) Energy levels involved in the double-Λ spontaneous four-wave mixing in ^{87}Rb. Solid blue and red arrows indicate cw pump and coupling fields, respectively. Wiggly blue and red arrows indicate generated Stokes and anti-Stokes fields. Black dots indicate initialization of atoms in the $F = 1$ hyperfine ground level. (b) Schematic of experimental setup. The pump and coupling beams have a waist of ≈ 0.85 mm. The collection spatial mode is focused on the atomic ensemble with a waist of 175 μm. Detectors D1 and D2 detect the Stokes field, and D3 and D4 the anti-Stokes fields in a Hanbury-Brown and Twiss like setup. $\lambda/2$: half-wave plate, $\lambda/4$: quarter-wave plate, PBS: polarizing beamsplitter, D1-D4: single photon detectors.

sition and the anti-Stokes photons have a frequency ω_a resonant to the $|5P_{1/2}, F' = 2\rangle \rightarrow |5S_{1/2}, F = 1\rangle$ transition (see Fig. 1(a)). The pump and coupling fields are circularly polarized, orthogonal to each other, and are directed at an elongated magneto-optical trap (MOT) of cold ^{87}Rb atoms, along the long axis in a counter-propagating configuration (Fig. 1(b)). The SFWM process begins by initializing atoms in the MOT into a state in the $|5S_{1/2}, F = 1\rangle$ hyperfine ground level via optical pumping. The MOT cooling beams are switched off during the SFWM measurement. The optical depth (OD) of the atomic cloud is ~ 30. The spatial modes for collecting the Stokes and anti-Stokes photons are focused on the atomic ensemble with a waist of 175 μm. The collection modes form an angle of 1° with the pump and coupling fields to reduce background scattering. Polarization filters and temperature-controlled etalon filters (bandwidth ≈100 MHz) are inserted in both Stokes and anti-Stokes collection arms to suppress unwanted photons. The photons collected in the Stokes and anti-Stokes arms are split using 50:50 fiber beamsplitters (BS) and detected using single photon detectors (D1-D4). A timestamp unit with 2 ns timing resolution records the photon arrival times in each of these four detectors. Second, third and fourth-order field correlations are analyzed using this data.

A single frequency conversion process produces the following output state that can contain multiple Stokes and anti-Stokes photons [28, 30–32]:

$$|\Psi\rangle = \frac{1}{\beta}\sum_{n=0}^{\infty}(\alpha)^n\,|n,n\rangle. \tag{1}$$

Here, $\beta \equiv \cosh\zeta$, $\alpha \equiv \tanh\zeta$, ζ depends on the strength of the pump, the nonlinear interaction, and the duration of interaction, and $|n,n\rangle$ indicates correlated Fock states with n photons each in the Stokes and anti-Stokes modes. A complete expression for the interaction Hamiltonian and the nonlinear susceptibilities can be found in [23, 33]. From Eq. (1), it is evident that at small interaction strengths ($\zeta \ll 1$) the probability of generating states with four photons (P_4) relates to the probability of producing pairs (P_2) as $P_4 = P_2^2$. In this case the four-photon state corresponds to two Stokes and two anti-Stokes photons that are correlated and entangled, generated within a single SFWM process [32]. Furthermore, this is twice the probability of four-photon states present if the output contains a Poissonian distribution of photons [32] (Supplementary Material).

In the following, we characterize the composition of correlated quadruplets versus uncorrelated double pairs from our source using higher-order intensity correlation measurements and verify the presence of twice as many correlated quadruplets as uncorrelated four-photons. We also compare rates of pair production versus four-photon production for varying pump powers.

We measure the second-order intensity correlations as a first step towards characterizing the statistical properties of the generated fields. The normalized second-order correlation between stationary fields $\hat{E}_i$ in mode i, detected at time t_i, and $\hat{E}_j$ detected at time $t_j = t_i + \tau_{ji}$ is [34]

$$g^{(2)}_{ji}(\tau_{ji}) = \frac{\langle \hat{E}_i^\dagger(t_i)\hat{E}_j^\dagger(t_i+\tau_{ji})\hat{E}_j(t_i+\tau_{ji})\hat{E}_i(t_i)\rangle}{\langle \hat{E}_j^\dagger(t_i+\tau_{ji})\hat{E}_j(t_i+\tau_{ji})\rangle\langle \hat{E}_i^\dagger(t_i)\hat{E}_i(t_i)\rangle}\,, \tag{2}$$

where $i, j \in \{s, a\}$ for the Stokes (s) and anti-Stokes (a) modes.

The second-order autocorrelations $g^{(2)}_{s,s}(\tau)$, $g^{(2)}_{a,a}(\tau)$ and cross-correlation $g^{(2)}_{s,a}(\tau)$ were measured for pump and coupling powers of about 800 μW and 10 mW, respectively, and a pump detuning of $\Delta_p = 2\pi \times 40$ MHz. Results are shown in Fig. 2. We infer a Stokes—anti-Stokes two photon correlation time of around 16 ns from the time constant of an exponentially decaying fit to the $g^{(2)}_{s,a}(\tau)$ results. The Stokes and anti-Stokes modes independently display thermal statistics as seen from their intensity autocorrelation at $\tau = 0$ (inset in Fig. 2).

We analyze the temporal distribution of coincidences

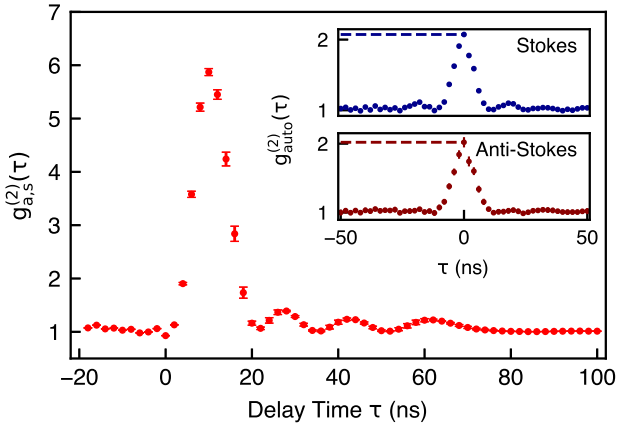

FIG. 2. Normalized second-order correlation measurements. Main figure: Stokes—anti-Stokes cross-correlation as a histogram of coincidences for various detection delays τ, normalized to the Stokes and anti-Stokes singles rates for a 2 ns bin size and an integration time of 150 s. Results averaged over 17 measurements. Oscillations are caused by the coupling field that drives the $|2\rangle \rightarrow |3\rangle$ transition at an effective Rabi frequency of $2\pi \times 55\,\mathrm{MHz}$. Insets: Unheralded autocorrelation measurements of Stokes photons (blue) with peak $g^{(2)}_{s,s}(0) = 2.07 \pm 0.02$ and anti-Stokes photons (red) with peak $g^{(2)}_{a,a}(0) = 2.02 \pm 0.07$ (jointly labeled $g^{(2)}_{\mathrm{auto}}(\tau)$).

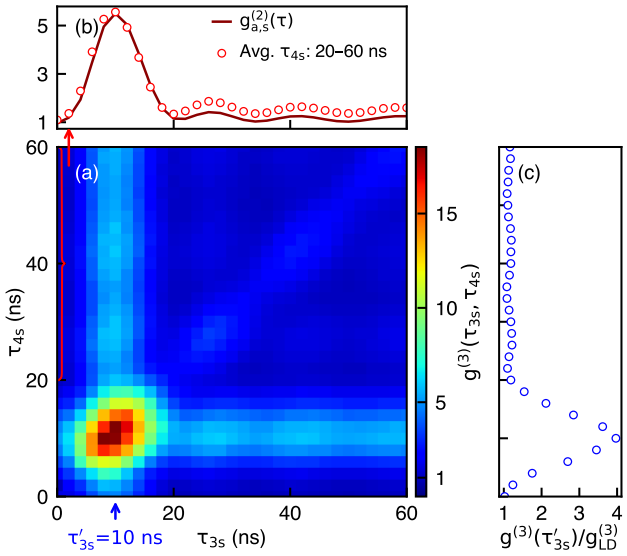

FIG. 3. Normalized third-order correlation. (a) Normalized triple coincidences $g^{(3)}_{a,a,s}$ for various delays τ_{3s} and τ_{4s} between a detection in D3 and D4, respectively, and a heralding Stokes photon in either of D1 or D2. Coincidences analyzed from data acquired over a measurement duration T_m of 0.7 h, normalized by the accidental triplet counts $R_s R_3 R_4 \delta t^2 T_m$, where the time bin $\delta t = 2$ ns, and R_i is the single count in detector Di. The $g^{(3)}_{a,a,s}$ peak value of 18 indicates strongly correlated triplets. (b) Comparison of the vertical ridge with $g^{(2)}_{a,s}$. Red dots: $g^{(3)}_{a,a,s}$ results averaged over τ_{4s} from 20 ns to 60 ns. Solid line: normalized cross-correlation $g^{(2)}_{a,s}(\tau_{3s})$ between a Stokes detection in D1 or D2 and an anti-Stokes detection in D3. (c) Peak to ridge ratio. Blue dots: Trace at $\tau_{3s} = 10$ ns, normalized by average $g^{(3)}$ value at $\tau_{3s} = 10$ ns and $\tau_{4s} = 20$ to 60 ns, i.e., $g^{(3)}_{\mathrm{LD}}$ at the limit of long delays outside of 20 ns coincidence window. The peak is close to 4 times the mean value in the ridge.

involving more than two detections to determine the ratio of correlated quadruplets to two independent pairs detected together by chance. Since there is no physical mechanism that generates states involving only three photons, a measurement of triplet coincidences involving two Stokes and one anti-Stokes photons or two anti-Stokes and one Stokes photon provides similar information to a four-fold coincidence measurement of two anti-Stokes and two Stokes photons, while being faster to acquire and simpler to visualize.

The normalized third-order correlation between the Stokes and anti-Stokes modes from two anti-Stokes detections at times t_3 and t_4 and a Stokes detection at time t_s is

$$g^{(3)}_{a,a,s}(t_3, t_4, t_s) = \frac{\langle \hat{E}^\dagger_s(t_s)\hat{E}^\dagger_a(t_3)\hat{E}^\dagger_a(t_4)\hat{E}_a(t_4)\hat{E}_a(t_3)\hat{E}_s(t_s)\rangle}{\langle \hat{E}^\dagger_s(t_s)\hat{E}_s(t_s)\rangle\langle \hat{E}^\dagger_a(t_3)\hat{E}_a(t_3)\rangle\langle \hat{E}^\dagger_a(t_4)\hat{E}_a(t_4)\rangle}, \quad (3)$$

where the numerator leads to the triple-coincidence rate $G^{(3)}_{a,a,s}(t_3, t_4, t_s)$. This can be expressed in terms of second-order correlations as shown in Eq. (7) in the Supplementary Material.

Figure 3 shows $g^{(3)}_{a,a,s}$ for triplets from an anti-Stokes detection each in D3 (at t_3) and D4 (at t_4), and a Stokes detection in either of D2 or D1 (at t_s), where the measurement was performed under the same conditions as the second order correlation measurements. The results are represented in terms of relative delays $\tau_{3s} = t_3 - t_s$ and $\tau_{4s} = t_4 - t_s$. The technique used to identify triplets from pair coincidences is described in the Supplementary Material.

The features in Fig. 3 can be understood intuitively or by analyzing Eq. (7) in the Supplementary Material over various delays. Given a coherence time Δt for the Stokes and anti-Stokes photons, when $\tau_{3s}, \tau_{4s}, \tau_{34} \gg \Delta t$, the triplet rate reduces to the background accidental rate in Fig. 3. When $\tau_{3s}, \tau_{4s} \gg \Delta t$ and $\tau_{34} \lesssim \Delta t$, the autocorrelation in the anti-Stokes mode dominates the result ($g^{(3)}_{a,a,s}(\tau_{3s}, \tau_{4s}, \tau_{34}) \rightarrow g^{(2)}_{a,a}(\tau_{34})$). In this case, the triplets are caused by the combination of an accidental click in the Stokes mode with a bunched thermal state in the anti-Stokes mode, forming the moderately bright diagonal in Fig. 3.

When $\tau_{3s}, \tau_{34} \gg \Delta t$ but $\tau_{4s} \lesssim \Delta t$ (horizontal ridge), or when $\tau_{4s}, \tau_{34} \gg \Delta t$ but $\tau_{3s} \lesssim \Delta t$ (vertical ridge), the strong cross-correlation between anti-Stokes (in D4

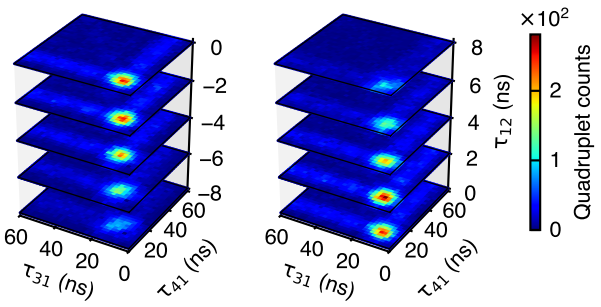

FIG. 4. Quadruple-coincidence detection. Each slice shows unnormalized four-fold coincidences from a detection in each of D1 to D4 for a fixed delay τ_{12} with a 2 ns time bin, and a range of delays τ_{31} and τ_{41}. Data acquired over a measurement duration of 0.7 h. The coincidences are peaked for $\tau_{12} = 0 \pm 2$ ns and τ_{31} and $\tau_{41} = 10 \pm 2$ ns.

or D3, respectively) and Stokes photon pairs are the dominant contributions. Here, the triplets are formed by a combination of a correlated Stokes—anti-Stokes pair with an uncorrelated additional photon in the anti-Stokes mode. Thus, the maximum mean value in the horizontal and vertical ridges at long delays is equal to $g^{(2)}_{s,a}(0)$ as seen in Fig. 3(b).

In the region where $\tau_{3s}, \tau_{34}, \tau_{4s} \lesssim \Delta t$ the coincidences increase several-fold. Theoretically, the peak is expected to be 4 times the average in either the horizontal or vertical ridges (at delays longer than Δt) when the output contains highly correlated four-photon states (refer to Supplementary Material). We see from Fig.3(c) that in our measurement, the $g^{(3)}_{a,a,s}$ peak is about four times the mean along the vertical ridge (outside the central 20 ns window). Thus, we are confident that the output of the SFWM process contains twice as many strongly correlated four-photons as uncorrelated double-pairs, that contribute to the high three-fold coincidences in the triplet measurement.

We search for four-fold coincidences between detections of two photons in the anti-Stokes mode and two photons in the Stokes mode for further analysis of four-photon states produced from our SFWM source. The normalized fourth-order cross-correlation is

$$g^{(4)}_{s,s,a,a}(t_1,t_2,t_3,t_4) = \frac{\langle \hat{E}^\dagger_a(t_4)\hat{E}^\dagger_a(t_3)\hat{E}^\dagger_s(t_2)\hat{E}^\dagger_s(t_1)\hat{E}_s(t_1)\hat{E}_s(t_2)\hat{E}_a(t_3)\hat{E}_a(t_4)\rangle}{\langle \hat{E}^\dagger_s(t_1)\hat{E}_s(t_1)\rangle\langle \hat{E}^\dagger_s(t_2)\hat{E}_s(t_2)\rangle\langle \hat{E}^\dagger_a(t_3)\hat{E}_a(t_3)\rangle\langle \hat{E}^\dagger_a(t_4)\hat{E}_a(t_4)\rangle}, \quad (4)$$

where the numerator gives $G^{(4)}_{s,s,a,a}(t_1,t_2,t_3,t_4)$: the quadruplet rate for coincidences from two Stokes detections at times t_1 and t_2 respectively and two anti-Stokes detections at time t_3 and t_4, respectively. We identify four-fold coincidences for detections at times t_1 to t_4 in detectors D1 to D4, under the same experimental conditions as used in previous measurements, with maximum delays up to 60 ns. We represent the data as sliced three dimensional histogram plots (see Fig. 4), where each slice shows quadruplets for a fixed delay τ_{12} and various relative delays τ_{31} and τ_{41}. We see the maximum density of quadruplets clustered around $\tau_{12} = 0 \pm 2$ ns and τ_{31} and $\tau_{41} = 8 \pm 2$ ns. Outside a 20 ns window centered at $(\tau_{12}, \tau_{31}, \tau_{41}) = (0\,\text{ns}, 10\,\text{ns}, 10\,\text{ns})$ the quadruplet count drops significantly, indicating the presence of highly-correlated quadruplets within 20 ns. The horizontal and vertical ridges in slices as τ_{12} approaches 0 arises from four-fold coincidences between accidentals and a correlated pair between D4-D1 or D3-D1, respectively. A relatively dull diagonal due to four-fold coincidences between accidentals and thermally bunched photons in D3-D4 can also be seen.

Due to the long coherence time of the Stokes and anti-Stokes photons, our triplet and quadruplet measurements are not limited by averaging effects due to detector resolution, which would have otherwise reduced the maximum of the triple and quadruple-coincidence peaks.

Next, we examine the pump power dependency of multiphoton states. Fig. 5(a) and (b) show the total rates of Stokes/anti-Stokes singles ($R_{s/a}$), pairs (R_p), triples (R_t), and quadruples (R_q), aggregated over all detector combinations, defined within a coincidence window of $t_c = 20$ ns and without subtraction of accidentals. Choosing t_c of 20 ns is appropriate as the detection of correlated double-pairs is peaked within this window as seen from the correlation measurements shown in Fig. 2.

A clear relationship between the pairs and quadruplets for increasing pump powers is better visualized in Fig. 5(c) and (d), where the R_p, R_t and R_q are shown relative to R_s and R_a, with axes in log scale. R_p scales approximately linearly with R_s and R_a. The slopes of R_t and R_q are both close to 2, which is expected from the fact that triplet and quadruplet photons originate from the same physical processes. Furthermore, these measurements indicate that the rate at which double pairs are detected scales close to quadratically with the rate of detecting photon-pairs. This confirms that the photons in the double pairs are produced from a higher-order process in frequency conversion. At a pump power of 800 μW, which is close to saturation, we detect pairs at the rate of $7.1(3) \times 10^4$ cps and quadruplets at the rate of 21(3) cps. We perform accidental subtraction to obtain a detection rate of 3(1) cps for truly correlated quadruplets. Based on the detection rates and characterization of optical losses, we infer a quadruple generation rate of $g_q = 2.5(4) \times 10^6$ cps and a pair generation rate of $g_p = 1.3(3) \times 10^7$ cps at this power. Details on the procedure for accidental subtraction, channel losses and inferring generation rate can be found in the Supplementary Material.

Summary – So far, narrowband multiphoton states have been demonstrated by spatially multiplexing two SFWM processes, spontaneous Raman events, and cascaded geometries [35–38]. Our results show that direct

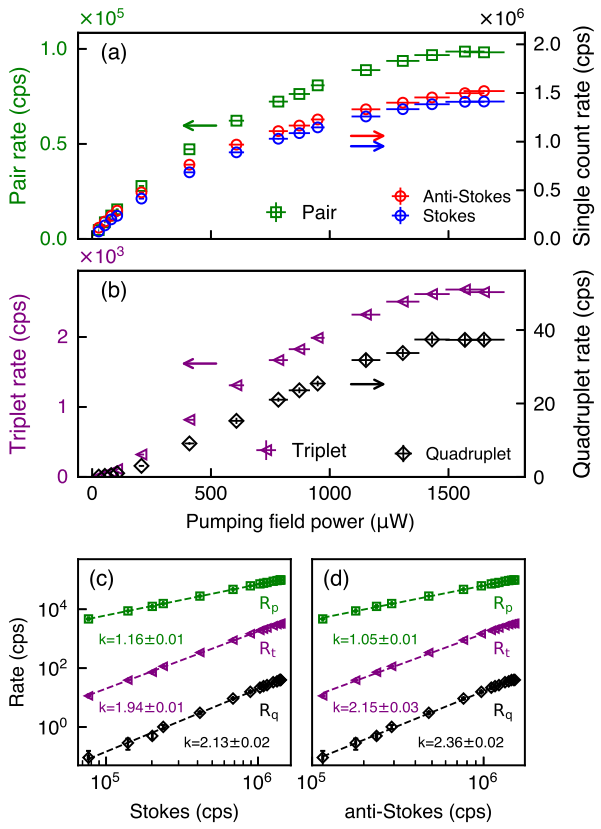

FIG. 5. Top: Detection rates as a function of pump power. (a) Single count rates (right axis) of Stokes (blue circles) and anti-Stokes photons (red circles), and photon pair rate (green squares, left axis) as functions of pump power. (b) Total photon triplet rates (magenta triangles, left axis) and photon quadruplet rate (black diamonds, right axis) as functions of pump power. Bottom: Ratio of pairs, triplets and quadruplets to singles. The photon pair rate R_p (green squares), photon triplet rate R_t (magenta triangles), and photon quadruplet rate R_q (black diamonds) from data in plots (a) and (b) represented in log-scale relative to the singles count rate R_s in Stokes mode (c) and singles count rate the anti-Stokes R_a (d). The change in singles count rates is achieved by varying the pump power while keeping all other parameters constant. The detuning of the pump is 40 MHz, while the coupling field is resonant with a fixed power of 10 mW. The atomic cloud has an OD ≈ 30.

pumping holds the potential to be a simpler alternative to producing multiphoton states. Furthermore, the correlated four photons generated here may potentially also be time-energy entangled [32, 39]. To our knowledge, microscopic models of SFWM as a collective process involving individual atomic emitters, have dealt only with the generation of photon-pairs [40, 41]. Our results pave the way for the extension of such models to better understand the microscopic origin of correlated multiphoton states, i.e., the physical origin of enhancement in the generation of a correlated second pair in the same mode as an initially generated pair. In the case of correlated four-photons generated from pulsed pumping of SPDC, such enhancement has been attributed to the bosonic nature of photons that leads to preferential bunching of otherwise indistinguishable photons into the same mode [14, 15, 32]. While this may explain our observations, there may be other contributions as well. The long coherence length of the generated photon-pairs in our experiment exceeds the length of the nonlinear medium and may potentially lead to stimulation of other pairs into the same mode, a process similar to the observations in [42]. We invite theoretical analyses of our experiment to explore the above processes and identify the underlying mechanism.

This research was supported by the National Research Foundation, Singapore and A*STAR under its CQT Bridging Grant, and through the Ministry of Education, Singapore through grant MOET32024-0009.

* christian.kurtsiefer@gmail.com

[1] J.-W. Pan, Z.-B. Chen, C.-Y. Lu, H. Weinfurter, A. Zeilinger, and M. Żukowski, Rev. Mod. Phys. **84**, 777 (2012).
[2] D. M. Greenberger, M. A. Horne, A. Shimony, and A. Zeilinger, American Journal of Physics **58**, 1131 (1990).
[3] J. W. Pan, D. Bouwmeester, M. Daniell, H. Weinfurter, and A. Zeilinger, Nature **403**, 515 (2000).
[4] H. Mikami, Y. Li, K. Fukuoka, and T. Kobayashi, Phys. Rev. Lett. **95**, 150404 (2005).
[5] W. Dür, G. Vidal, and J. I. Cirac, Phys. Rev. A **62**, 062314 (2000).
[6] M. Hillery, V. Bužek, and A. Berthiaume, Phys. Rev. A **59**, 1829 (1999).
[7] Y.-A. Chen, A.-N. Zhang, Z. Zhao, X.-Q. Zhou, C.-Y. Lu, C.-Z. Peng, T. Yang, and J.-W. Pan, Phys. Rev. Lett. **95**, 200502 (2005).
[8] M. Mitchell, J. Lundeen, and A. Steinberg, Nature **429**, 161 (2004).
[9] R. Raussendorf and H. J. Briegel, Phys. Rev. Lett. **86**, 5188 (2001).
[10] D. E. Browne and T. Rudolph, Phys. Rev. Lett. **95**, 010501 (2005).
[11] M. Bourennane, M. Eibl, S. Gaertner, C. Kurtsiefer, A. Cabello, and H. Weinfurter, Phys. Rev. Lett. **92**, 107901 (2004).
[12] L.-B. Deng, L.-Z. Zhang, and S.-G. Sun, Journal of Modern Optics **40**, 169 (1993).
[13] J. Tiedau, T. J. Bartley, G. Harder, A. E. Lita, S. W. Nam, T. Gerrits, and C. Silberhorn, Phys. Rev. A **100**, 041802 (2019).
[14] H. Weinfurter and M. Żukowski, Phys. Rev. A **64**, 010102 (2001).
[15] M. Eibl, S. Gaertner, M. Bourennane, C. Kurtsiefer, M. Żukowski, and H. Weinfurter, Phys. Rev. Lett. **90**, 200403 (2003).
[16] N. Kiesel, M. Bourennane, C. Kurtsiefer, H. Weinfurter, D. Kaszlikowski, W. Laskowski, and M. Zukowski, Journal of Modern Optics **50**, 1131 (2003).

[17] S. Bettelli, Physical Review A **81**, 037801 (2010).

[18] M. Razavi, I. Söllner, E. Bocquillon, C. Couteau, R. Laflamme, and G. Weihs, Journal of Physics B: Atomic, Molecular and Optical Physics **42**, 114013 (2009).

[19] J.-S. Shiu, Z.-Y. Liu, C.-Y. Cheng, Y.-C. Huang, I. A. Yu, Y.-C. Chen, C.-S. Chuu, C.-M. Li, S.-Y. Wang, and Y.-F. Chen, Phys. Rev. Res. **6**, L032001 (2024).

[20] J.-M. Chen, C.-Y. Hsu, W.-K. Huang, S.-S. Hsiao, F.-C. Huang, Y.-H. Chen, C.-S. Chuu, Y.-C. Chen, Y.-F. Chen, and I. A. Yu, Phys. Rev. Res. **4**, 023132 (2022).

[21] J. K. Thompson, J. Simon, H. Loh, and V. Vuletić, Science **313**, 74 (2006).

[22] S. Du, P. Kolchin, C. Belthangady, G. Y. Yin, and S. E. Harris, Physical Review Letters **100**, 183603 (2008).

[23] S. Du, J. Wen, and M. H. Rubin, J. Opt. Soc. Am. B **25**, C98 (2008).

[24] P. Kolchin, Physical Review A **75**, 033814 (2007).

[25] B. Srivathsan, G. K. Gulati, C. M. Y. Brenda, G. Maslennikov, D. Matsukevich, and C. Kurtsiefer, Physical Review Letters **111**, 123602 (2013).

[26] V. Balić, D. A. Braje, P. Kolchin, G. Y. Yin, and S. E. Harris, Physical Review Letters **94**, 183601 (2005).

[27] H. J. Kimble, Nature **453**, 1023 (2008).

[28] N. Sangouard, C. Simon, H. De Riedmatten, and N. Gisin, Reviews of Modern Physics **83**, 33 (2011).

[29] P. Kolchin, S. Du, C. Belthangady, G. Y. Yin, and S. E. Harris, Physical Review Letters **97**, 113602 (2006).

[30] U. Leonhardt, Reports on Progress in Physics **66**, 1207 (2003).

[31] A. I. Lvovsky, Squeezed light, in *Photonics* (John Wiley & Sons, Ltd, 2015) Chap. 5, pp. 121–163.

[32] H. de Riedmatten, V. Scarani, I. Marcikic, A. Acin, W. Tittel, H. Zbinden, and N. Gisin, Journal of Modern Optics **51**, 1637 (2004), quant-ph/0310167.

[33] J. Wen and M. H. Rubin, Physical Review A **74**, 023808 (2006).

[34] R. J. Glauber, Physical Review **130**, 2529 (1963).

[35] M.-X. Dong, W. Zhang, Z.-B. Hou, Y.-C. Yu, S. Shi, D.-S. Ding, and B.-S. Shi, Optics Letters **42**, 4691 (2017).

[36] J. Park and H. S. Moon, Applied Physics Letters **120**, 024001 (2022).

[37] Y. Wu, L. Tian, Z. Xu, W. Ge, L. Chen, S. Li, H. Yuan, Y. Wen, H. Wang, C. Xie, and K. Peng, Phys. Rev. A **93**, 052327 (2016).

[38] H. Hübel, D. R. Hamel, A. Fedrizzi, S. Ramelow, K. J. Resch, and T. Jennewein, Nature **466**, 601 (2010).

[39] K.-K. Park, J.-H. Kim, T.-M. Zhao, Y.-W. Cho, and Y.-H. Kim, Optica **4**, 1293 (2017).

[40] C. H. Raymond Ooi, Q. Sun, M. S. Zubairy, and M. O. Scully, Physical Review A **75**, 013820 (2007).

[41] Y. Jiang, Y. Mei, and S. Du, Physical Review A **107**, 053703 (2023).

[42] A. Lamas-Linares, J. Howell, and D. Bouwmeester, Nature **412**, 887 (2001).